Journal of Power Sources 235 (2013) 187–192

Contents lists available at SciVerse ScienceDirect

Journal of Power Sources

journal homepage: www.elsevier.com/locate/jpowsour

# Highly uniform deposition of $MoO_3$ nanodots on multiwalled carbon nanotubes for improved performance of supercapacitors

Qasim Mahmood [a], Hyung Joong Yun [b], Woo Sik Kim [a,*], Ho Seok Park [a,*]

[a] Department of Chemical Engineering, College of Engineering, Kyung Hee University, 1 Seochon-dong, Giheung-gu, Youngin-si, Gyeonggi-do 446-701, Republic of Korea
[b] Division of Material Science, Korea Basic Science Institute (KBSI), Daejeon 305806, Republic of Korea

## HIGHLIGHTS

- The $MoO_3$ nanodots were uniformly deposited on MWCNTs through a sonochemical method.
- The specific capacitance was significantly improved by the deposition of $MoO_3$.
- $MoO_3$/MWCNT hybrids showed a good rate capability and cyclic stability.
- The energy density of $MoO_3$/MWCNT hybrids was 38.7 Wh/kg using organic electrolyte.

## ARTICLE INFO

*Article history:*
Received 29 November 2012
Received in revised form
25 January 2013
Accepted 29 January 2013
Available online 9 February 2013

*Keywords:*
Carbon nanotube
Molybdenum oxide
Hybrid
Sonochemistry
Supercapacitors

## ABSTRACT

We demonstrate the sonochemical synthesis of multiwalled carbon nanotubes (MWCNTs) and $MoO_3$ hybrids for an application in supercapacitor (SC) electrodes. The $MoO_3$ nanodots with the diameter of $<10$ nm are uniformly deposited on the surfaces of MWCNTs as characterized by TEM and STEM images. The specific capacitance of 103 F $g^{-1}$ in $MoO_3$/MWCNT hybrids is two times higher than 42 F $g^{-1}$ of the pristine MWCNTs and four times higher than 22 F $g^{-1}$ of $MoO_3$. Moreover, hybrid electrodes show a good rate capability of $>90\%$ retention up to 2.12 A $g^{-1}$ and cyclic stability of 80% retention during 1000 cycles of charge/discharge because of the mechanical stability of the MWCNTs and the good contact between the $MoO_3$ and MWCNTs. The energy density of $MoO_3$/MWCNT hybrids is evaluated to be 38.7 Wh $kg^{-1}$ by using an organic electrolyte. Therefore, the hybridization of MWCNTs and redox-active $MoO_3$ nanodots provides a rational design strategy to overcome the critical challenges of pseudocapacitors such as poor rate and cycle stability, while improving the low specific capacitance of electric double layer capacitors (EDLCs).



## 1. Introduction

Carbon nanotubes (CNTs) have been considered as an attractive SC electrode materials due to their good electrical conductivity, high surface area, chemical and mechanical stability, and large accessible mesopores [1–7]. The specific capacitances of CNTs were mostly limited to below 100 F $g^{-1}$ [8,9], because they store charges at the electrical double layer through a non-faradaic process [10–12]. To enhance the specific capacitance for high energy density, the functionalization of CNTs and their composites with redox-active or pseudocapacitive materials has recently been explored [13,14]. In particular, the deposition of various redox-active metal oxides (MOs), including $RuO_2$, $MnO_2$, $Ni(OH)_2$, $Co_3O_4$, $Fe_2O_3$, $In_2O_3$, $TiO_2$, and $V_2O_5$ on the surface of CNTs has been extensively investigated [15–20]. Such an approach is expected to overcome the critical challenges related to MOs, such as poor rate and cycle stability due to their low electrical conductivity and volume expansion, while improving the low specific capacitance of CNTs.

Herein, we demonstrate the sonochemical synthesis of $MoO_3$/MWCNT hybrids for an application in SCs. Although $MoO_3$ was used as the energy storage material due to its unique structural anisotropy and redox behavior [21–24], there are very few reports on the application of $MoO_3$/MWCNT hybrids in SC electrodes. Moreover, the rate and cycle performances of $MoO_3$ are still a bottleneck for practical power applications. The integration of redox-active $MoO_3$ allows CNTs to achieve good rate and cycle performances while improving the specific capacitance.

* Corresponding authors. Tel.: +82 31 201 3327.
*E-mail address:* phs0727@khu.ac.kr (H.S. Park).

0378-7753/$ – see front matter 
http://dx.doi.org/10.1016/j.jpowsour.2013.01.165

## 2. Experimental section

### 2.1. Synthesis of $MoO_3$/MWCNT hybrids

$MoO_3$/MWCNT nanodot hybrids were synthesized by a sonochemical method. $MoCl_5$ powder was used as a precursor material for $MoO_3$. In a typical synthesis procedure, 0.4 g $MoCl_5$ was homogenously mixed with 6 mL of ethanol, followed by the addition of 30 mg of MWCNTs. The mixture was constantly stirred until a homogeneous solution was obtained. This solution was sonicated for 2 h while at the same time, 6 mL of deionized (DI) water was added. The solution was left to stand for 24 h and the resulting materials were washed with DI water several times and then dried in an oven before characterization and electrochemical testing. For a control sample, $MoO_3$ was synthesized by sol–gel method through hydrolysis and condensation of $MoCl_5$.

### 2.2. Electrochemical measurements

The electrochemical behavior of the SC devices was evaluated at room temperature via cyclic voltammetry (CV). CV measurements were obtained using a three-electrode system with the active material on an aluminum sheet substrate as the working electrode, platinum wire as the counter electrode, and Ag/AgCl as the reference electrode. The working electrode was composed of 85 wt% active material and 15 wt% PVDF as a binder. These two components were mixed using a few drops of NMP as a solvent, grounded in an agate mortar until a homogenous paste was obtained, and then pasted on a conductive aluminum sheet substrate. The electrode was dried overnight in an oven at 80 °C and then cut into a 0.5 × 0.5 $cm^2$ area for use as a working electrode. Galvanostatic charge/discharge (GCD) curves, rate capability, and cycle stability were measured with two electrode configuration. In all measurements, 1 M lithium perchlorate ($LiClO_4$) in propylene carbonate (PC) was used as the electrolyte.

### 2.3. Instrumental methods

Scanning Electron Microscope (SEM) images were obtained by a Field Emission SEM (Philips SEM 535M) equipped with schottky based field emission gun. Transmission electron microscope (TEM) images were obtained with a JEM-3010 high-resolution transmission electron microscope (HR TEM, 300 kV). X-ray diffraction (XRD) data were obtained in the range of $2\theta = 2–50°$ using a Rigaku D/max lllC (3 kW) with a θ/θ goniometer equipped with a Cu K radiation generator. Thermogravimetric analysis (TGA) was carried out using a DuPont 2200 thermal analysis station. TGA data were collected at a heating rate of 10 °C $min^{-1}$ in nitrogen. The X-ray photoelectron spectroscopy (XPS) data were obtained using a Thermo MultiLab 2000 system. An Al Mg α X-ray source at 200 W was used with pass energy of 20 eV and a 45° takeoff angle under a $10^{-7}$ Torr vacuum analysis chamber. The electrochemical characteristics of the SC devices were evaluated by CV curves obtained on a CHI 760D electrochemical workstation (CH Instruments) at room temperature. In addition, galvanostatic charge/discharge measurements were acquired using an IVIUMSTAT electrochemical interface device.

## 3. Results and discussion

The morphologies of $MoO_3$/MWCNT hybrids were investigated by using FESEM and TEM as shown in Fig. 1. The small-sized $MoO_3$

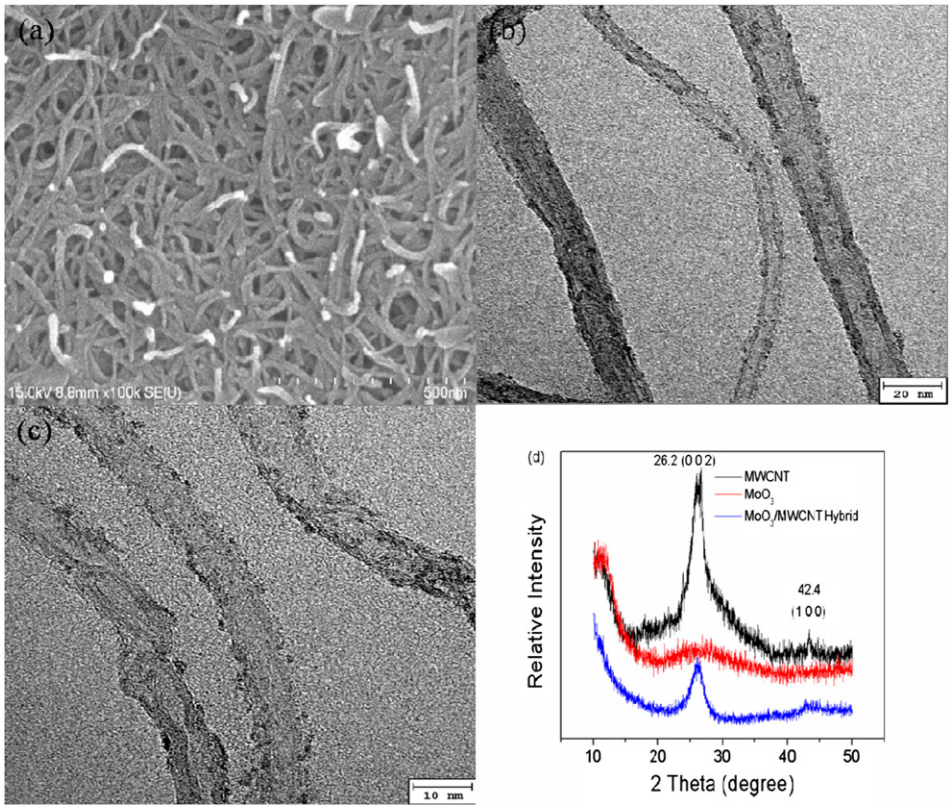


**Fig. 1.** (a) FESEM image of $MoO_3$/MWCNT hybrid, (b) and (c) TEM images of $MoO_3$/MWCNT hybrid at different scales, (d) XRD of $MoO_3$/MWCNT hybrid, MWCNT and $MoO_3$.

nanodots on the surface of the MWCNTs could not be clearly observed by FESEM due to resolution limitations. However, a uniform coating and dispersion of $MoO_3$ nanodots on the surface of MWCNTs without any discernible aggregation was shown in the TEM images of the hybrids. The size of the $MoO_3$ nanodots ranged from 2 to 10 nm. From the high-resolution TEM image, no fringes from $MoO_3$ were observed, thus indicating the amorphous nature of $MoO_3$ on the surface of the MWCNTs. $MoO_3$ as a control sample was synthesized through a sol–gel process under the same experimental conditions as those employed for the $MoO_3$/MWCNT hybrids. $MoO_3$ showed an irregular morphology with amorphous nature as shown in TEM image (see Fig. S1). XRD spectra confirmed that the as synthesized $MoO_3$ in the hybrids was amorphous, as no peaks corresponding to $MoO_3$ were detected. The pristine MWCNTs and $MoO_3$/MWCNT hybrids showed two peaks at $2\theta = 26.2^\circ$ and $42.4^\circ$ corresponding to the (002) and (100) planes, of the MWCNTs, respectively [25]. The reduction in peak intensity and the existence of peak broadening in the $MoO_3$/MWCNT hybrids relative to those of pristine MWCNTs were attributed to the composition of the coated $MoO_3$ nanodots [26,27].

The presence and distribution of $MoO_3$ on the MWCNTs were observed by STEM images in Fig. 2. As shown in the apparent contrast discrepancy in the dark field TEM image, $MoO_3$ nanodots were clearly deposited on the MWCNT surfaces. The existence of $MoO_3$ nanodots was confirmed by the mapping of Mo and O signals. The coating of $MoO_3$ nanodots on the surface of the MWCNTs was so stable that the morphology of the hybrid remained intact even after high power sonication for the preparation of TEM samples. The uniform distribution and composition of the $MoO_3$ nanodots in the hybrid was evaluated by energy dispersive X-ray spectroscopy (EDX), TGA, and XPS (see Fig. S2–4). The atomic ratio of Mo to O was measured to be 1:3, corresponding to the chemical composition of $MoO_3$. From TGA curves of pristine MWCNTs and $MoO_3$/MWCNT hybrids, the amount of $MoO_3$ in the hybrids was calculated to be ~20 wt%. The pristine MWCNTs did not exhibit any decomposition up to 1000 °C in a nitrogen atmosphere, while a weight loss of ~16 wt% was observed in the $MoO_3$/MWCNT hybrids up to 380 °C due to the removal of physisorbed and chemisorbed water. An additional ~3 wt% weight loss occurred in the range of 380–500 °C because of the transformation of amorphous $MoO_3$ into crystalline form. Finally, ~20 wt% of the $MoO_3$ decomposed around 800 °C [28–30]. Since the loading of $MoO_3$ above 20 wt% lead to aggregation into a large particle, the specific capacitance can be deteriorated [31]. The influence of $MoO_3$ loading on the capacitor performance will be discussed later. The $Mo^{6+}$ oxidation state of Mo and chemical identity of the hybrid was confirmed by the XPS survey spectra [32,33].

The electrochemical behavior and capacitor performance of the electrodes were evaluated by CV and GCD measurements as shown in Fig. 3. For the electrochemical measurements, 1 M of $LiClO_4$ in PC was chosen as the electrolyte. The CV curve for the pristine MWCNTs exhibited a rectangular shape corresponding to ideal EDLC at a scan rate of 100 mV $s^{-1}$. In contrast, the $MoO_3$/MWCNT hybrids showed tilted behavior, which indicates the faradic process

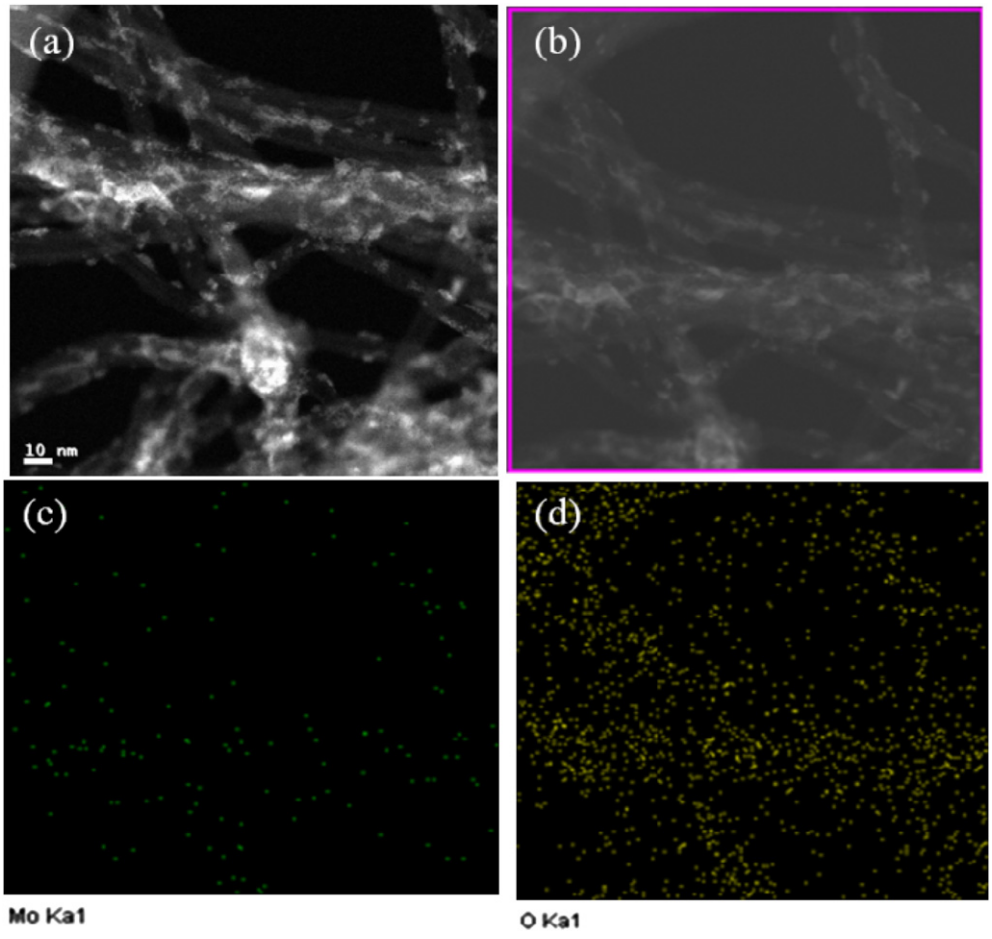


**Fig. 2.** (a) Dark field TEM image of $MoO_3$/MWCNT hybrid, (b) STEM image, (c) and (d) Mo and O mapping images in the $MoO_3$/MWCNT hybrid.

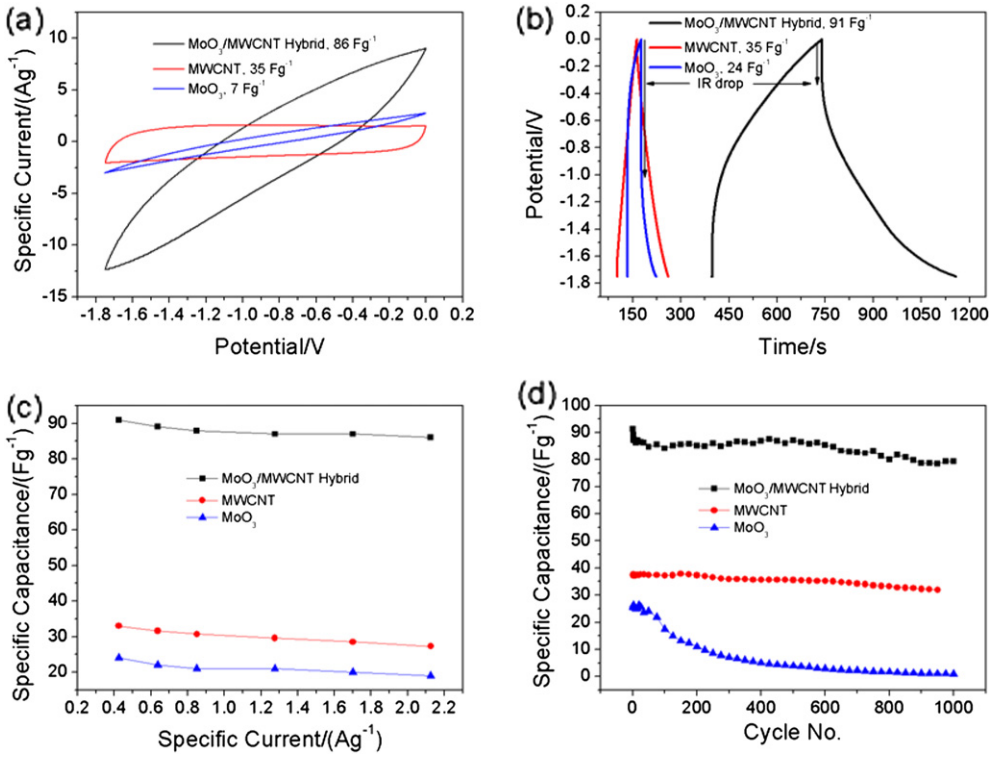


**Fig. 3.** (a) CV curves of $MoO_3$/MWCNT hybrid, MWCNT and $MoO_3$ at a scan rate of 100 mV $s^{-1}$, (b) Galvanostatic charge/discharge curves of $MoO_3$/MWCNT hybrid, MWCNT and $MoO_3$ at a current rate of 0.42 A $g^{-1}$, (c) Rate capability comparison of $MoO_3$/MWCNT hybrid, MWCNT and $MoO_3$, (d) Cycle stability comparison of $MoO_3$/MWCNT hybrid, MWCNT and $MoO_3$.

of MOs for additional charge storage, as well as EDLC. However, no discernible redox wave was found even for pristine $MoO_3$, indicating the existence of amorphous $MoO_3$ (see Fig. S5). Three samples exhibited similar behavior at different scan rates. As the scan rate decreased from 100 mV $s^{-1}$ to 25 mV $s^{-1}$, the specific capacitances of the $MoO_3$/MWCNT hybrids were enhanced from 86 F $g^{-1}$ to 103 F $g^{-1}$ (see Fig. S6) [34]. The maximum specific capacitance of 103 F $g^{-1}$ observed in this measurement range was two times higher than 42 F $g^{-1}$ capacitance of the pristine MWCNTs and four times higher than the 22 F $g^{-1}$ capacitance of $MoO_3$. Considering that the capacitance performance strongly depends upon the size of particles because a charge storage site is proportional to accessible surface area, the $MoO_3$ nanodots with the size of <10 nm were superior to the bulk $MoO_3$ for energy storage applications. Consequently, the improvement of the specific capacitance was attributed to the uniform deposition of $MoO_3$ nanodots on the surface of the MWCNTs and the synergistic hybridization of MWCNT conductive networks and $MoO_3$ [15–24].

To further study the capacitive performance of the $MoO_3$/MWCNT hybrids, the specific capacitances at a constant current of 0.42 A $g^{-1}$ were obtained from GCD curves using the following equation:

$$C = \frac{I}{\left[m\left(\frac{\Delta V}{\Delta t}\right)\right]} \quad (1)$$

where $I$ is the constant current at which the GCD curves were obtained, $m$ is the electrode mass, and $\Delta V/\Delta t$ is the slope of the discharge curve. Two electrodes were configured here to describe a real system. The pristine MWCNTs showed typical EDLC behavior in the form of a symmetric curve [35,36]. In contrast, the $MoO_3$ presented a large IR drop in the discharge curve due to its low electronic conductivity and the resistive effect of the binder material. The IR drop of the $MoO_3$/MWCNT hybrid decreased because of the good electrical properties of the MWCNTs. Furthermore, the specific capacitance increased due to the uniform deposition of $MoO_3$ nanoparticles on the MWCNTs, which would offer a high surface area and intimate interaction between the $MoO_3$ and MWCNTs. This behavior is usually observed for the nanoscale hybridization of carbon and MO materials, which results in the synergistic effects of hybrid materials in energy storage applications [37–39]. The GCD curves of the $MoO_3$/MWCNT hybrid, pristine MWCNTs, and pristine $MoO_3$ were compared at different specific currents of 0.63, 0.85, and 1.27 A $g^{-1}$. The specific capacitances were reduced with the increase in specific current, while the IR drops were enhanced because of the increase in the internal resistance at the high current value (see Fig. S7). The highest specific capacitance calculated from the GCD curves was 91 F $g^{-1}$ for the $MoO_3$/MWCNT hybrid, which was two times higher than the 35 F $g^{-1}$ value for pristine MWCNTs and three times higher than the 24 F $g^{-1}$ value for $MoO_3$. These results are in a good agreement with the CV findings despite the small discrepancy in the values due to the different measurement conditions and cell configurations.

Rate capability and cycle stability is an important parameter for practical applications of energy storage. All samples showed a good rate capability of >90% retention up to 2.12 A $g^{-1}$. In particular, $MoO_3$/MWCNT hybrids retained a high rate capability while enhancing the specific capacitance of MWCNT. The cyclic stabilities of MWCNT, $MoO_3$, and the $MoO_3$/MWCNT hybrid were measured with GCD curves obtained for 1000 cycles. The cyclic performance of the $MoO_3$ dramatically improved to 80% retention by hybridization with MWCNTs. This improvement was attributed to the mechanical stability of the MWCNTs and the good contact between

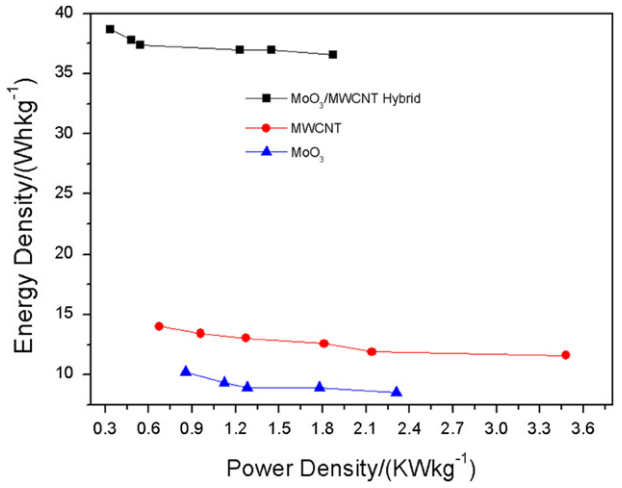


**Fig. 4.** Ragone plot for $MoO_3$/MWCNT hybrid, MWCNT and $MoO_3$ SCs.

the $MoO_3$ and MWCNTs. When as the amount of $MoO_3$ increased up to 30 wt%, the specific capacitance of hybrid increased up to 136 F $g^{-1}$. However, the cycle stability decreased down to 62% of the initial value due to structural deformation of high loading of $MoO_3$ and slow electron transfer kinetics during cycling process (see Fig. S8).

A Ragone plot of the energy density vs. the power density is an efficient way to evaluate the performance of energy storage devices. The energy density and power density of a SC can be calculated from the following equations [40]:

$$E = \frac{0.5\ CV^2}{3.6} \tag{2}$$

$$P = E\left[\frac{3600}{t}\right] \tag{3}$$

where $C$ is the specific capacitance in F $g^{-1}$, $V$ is the voltage window, and $t$ is the discharge time in seconds. From equation (2), it is clear that an increase in the capacitance or voltage window leads to an increase in the energy density. The voltage window can be increased through the use of a non-aqueous electrolyte (e.g., organic or ionic liquid electrolyte) [35,36]. Therefore, we used organic 1 M $LiClO_4$ in propylene carbonate as an electrolyte. As shown in Fig. 4, the maximum energy density reached to 38.7 Wh $kg^{-1}$ for $MoO_3$/MWCNT hybrids with a reasonable power density of 0.333 kW $kg^{-1}$. At a power density of 1.2 kW $kg^{-1}$, the energy density of the hybrid was 37 Wh $kg^{-1}$, which was higher than 13 and 9 Wh $kg^{-1}$ obtained for MWCNT and $MoO_3$, respectively. The maximum power density of the $MoO_3$/MWCNT hybrid was approached to 1.87 kW $kg^{-1}$ with an energy density of 36.57 Wh $kg^{-1}$. Ragone plot obtained from our work showed values that were comparable to previous results for CNT and CNT/MO hybrids [35–39]. The enhancement of energy density while maintaining the power density was due to the large potential window of the organic Li electrolyte, as well as the high capacitance of the $MoO_3$/MWCNT hybrid.

## 4. Conclusion

In conclusion, MWCNTs were uniformly deposited by $MoO_3$ nanodots with the diameter of <10 nm via a sonochemical method. The distribution and chemical composition of hybrids were confirmed by TEM, STEM mapping, XRD, TGA, and XPS spectroscopy. The $MoO_3$/MWCNT hybrids showed the greater capacitor performance compared to MWCNT and bulk $MoO_3$ due to the synergistic nanoscale hybridization. In particular, the hybrids revealed the maximum energy density of 38.7 Wh $kg^{-1}$ with a reasonable power density of 0.333 kW $kg^{-1}$, while the maximum power density of 1.87 kW $kg^{-1}$ with an energy density of 36.57 Wh $kg^{-1}$. The integration of MWCNT conductive networks and $MoO_3$ nanodots enabled to improve the cycle stability and rate capability while enhancing the energy density. Therefore, this research offers the rational design strategy of advanced electrode materials on a basis of the nanoscale hybridization of CNTs and MOs with the well-defined nanostructures for future applications in energy conversion and storage.

## Acknowledgments

We acknowledge the financial support by both the National Research Foundation (NRF) funded by the Korean Government (MEST) (20090063004) and NRF-2010-C1AAA001-0029018 and NRF Mid-career researcher program (NRF 2010-0017993).

## Appendix A. Supplementary data

Supplementary data related to this article can be found at http://dx.doi.org/10.1016/j.jpowsour.2013.01.165.

## References

[1] P. Simon, Y. Gogotsi, Nat. Mater. 7 (2008) 845.
[2] Y. Zhai, Y. Dou, D. Zhao, P.F. Fulvio, R.T. Mayes, S. Dai, Adv. Mater. 23 (2011) 4828.
[3] E. Frackowiak, Phys. Chem. Chem. Phys. 9 (2007) 1774.
[4] E. Frackowiak, F. Beguin, Carbon 39 (2001) 237.
[5] A.C. Dillon, Chem. Rev. 110 (2010) 6856.
[6] L.L. Zhang, X.S. Zhao, Chem. Soc. Rev. 38 (2009) 2520.
[7] E. Frackowiak, F. Beguin, Carbon 40 (2002) 1775.
[8] D.R. Rolison, J.W. Long, J.C. Lytle, A.E. Fischer, C.P. Rhodes, T.M. McEvoy, M.E. Bourg, A.M. Lubers, Chem. Soc. Rev. 38 (2009) 226.
[9] K. Naoi, P. Simon, Electrochem. Soc. Interface (2008) 34.
[10] J.R. Miller, P. Simon, Science 321 (2008) 651.
[11] D.S. Su, R. Schlogl, ChemSusChem 3 (2010) 136.
[12] A.S. Arico, P. Bruce, B. Scrosati, J.M. Tarascon, W.V. Schalkwijk, Nat. Mater. 4 (2005) 366.
[13] G. Lota, K. Fic, E. Frackowiak, Energy Environ. Sci. 4 (2011) 1592.
[14] A. Ghosh, Y.H. Lee, ChemSusChem 5 (2012) 480.
[15] H. Pan, J. Li, Y.P. Feng, Nanoscale Res. Lett. 5 (2010) 654.
[16] W.D. Zhang, B. Xu, L.C. Jiang, J. Mater. Chem. 20 (2010) 6383.
[17] C.Z. Yuan, B. Gao, L.F. Shen, S.D. Yang, L. Hao, X.J. Lu, F. Zhang, L.J. Zhang, X.G. Zhang, Nanoscale 3 (2011) 529.
[18] S.L. Candelaria, Y. Shao, W. Zhou, X. Li, J. Xiao, J.G. Zhang, Y. Wang, J. Liu, J. Li, G. Cao, Nano Energy 1 (2012) 195.
[19] L.J. Fu, H. Liu, C. Li, Y.P. Wu, E. Rahm, R. Holze, H.Q. Wu, Solid State Sci. 8 (2006) 113.
[20] W.X. Feng, W.D. Zhi, L. Ji, Acta Phys. Chim. Sin. 19 (2003) 509.
[21] L. Mai, B. Hu, W. Chen, Y. Qi, C. Lao, R. Yang, Y. Dai, Z.L. Wang, Adv. Mater. 19 (2007) 3712.
[22] A.V. Murugan, A.K. Viswanath, J. Appl. Phys. 100 (2006) 074319.
[23] T. Brezesinski, J. Wang, S.H. Tolbert, B. Dunn, Nat. Mater. 9 (2010) 146.
[24] L. Zheng, Y. Xu, D. Jin, Y. Xie, J. Mater. Chem. 20 (2010) 7135.
[25] D.N. Futaba, K. Hata, T. Yamada, T. Hiraoka, Y. Hayamizu, Y. Kakudate, O. Tanaike, H. Hatori, M. Yumura, S. Iijima, Nat. Mater. 5 (2006) 987.
[26] C. Yuan, L. Chen, B. Gao, L. Su, X. Zhang, J. Mater. Chem. 19 (2009) 246.
[27] H. Xia, Y. Wang, J. Lin, L. Lu, Nanoscale Res. Lett. 7 (2012) 33.
[28] R.F. de Farias, M.S. Refat, H.A. Hashem, J. Incl. Phenom. Macrocycl. Chem. 61 (2008) 113.
[29] J.M. Vivar, T. Lopez, A. Campero, Langmuir 7 (1991) 704.
[30] W. Dong, B. Dunn, J. Mater. Chem. 8 (1998) 665.
[31] I. Shakir, M. Shahid, S. Cherevko, C.H. Chung, D.J. Kang, Electrochim. Acta 58 (2011) 76.
[32] B.M. Reddy, B. Chowdhury, E.P. Reddy, A. Fernandez, Appl. Catal. A: Gen. 213 (2001) 279.
[33] J.G. Choi, L.T. Thompson, Appl. Surf. Sci. 93 (1996) 143.

[34] K. Okamura, R. Inoue, T. Sebille, K. Tomono, M. Nakayama, J. Electrochem. Soc. 158 (2011) A711.
[35] S.W. Lee, N. Yabuuchi, B.M. Gallant, S. Chen, B.S. Kim, P.T. Hammond, Y.S. Horn, Nat. Nanotech 5 (2010) 531.
[36] C. Liu, Z. Yu, D. Neff, A. Zhamu, B.Z. Jang, Nano Lett. 10 (2010) 4863.
[37] C. Guan, J. Liu, C. Cheng, H. Li, X. Li, W. Zhou, H. Zhang, H.J. Fan, Energy Environ. Sci. 4 (2011) 4496.
[38] X. Xia, Q. Hao, W. Lei, W. Wang, H. Wang, X. Wang, J. Mater. Chem. 22 (2012) 8314.
[39] A.S. Raut, C.B. Parker, J.T. Glass, J. Mater. Res. 25 (2010) 1500.
[40] J. Zhang, J. Jiang, H. Li, X.S. Zhao, Energy Environ. Sci. 4 (2011) 4009.